



**Search for $ZH \rightarrow e^+e^-b\bar{b}$ and $ZH \rightarrow \mu^+\mu^-b\bar{b}$ Production in 4.2 fb^{-1}
of data with the DØ Detector in $p\bar{p}$ Collisions at $\sqrt{s} = 1.96 \text{ TeV}$**

The DØ Collaboration
URL <http://www-d0.fnal.gov>
(Dated: March 12, 2009)

We report on a search for Standard Model Higgs boson (H) production in association with a Z boson in 4.2 fb^{-1} of $p\bar{p}$ collisions at $\sqrt{s} = 1.96 \text{ TeV}$ at the Fermilab Tevatron Collider. Events containing a reconstructed $Z \rightarrow e^+e^-$ or $Z \rightarrow \mu^+\mu^-$ candidate and two jets including at least one b -tagged jet are considered. The observed data are consistent with the expected Standard Model background. 95% CL upper limits on the ZH production cross section are set for Higgs masses (M_H) between 100 and 150 GeV. The limit for the full Run II dataset is 9.1 times the Standard Model prediction for $M_H = 115 \text{ GeV}$.

Preliminary Results for the 2009 Winter Conferences

I. INTRODUCTION

The Standard Model predicts a Higgs Boson as the residual field after the spontaneous breaking of the electroweak gauge symmetry, which produces a massless photon but massive W and Z bosons. The Higgs, which has so far eluded detection, would complete a remarkable list of experimentally confirmed Standard Model predictions. In the Standard Model, the Higgs production and branching fractions are functions of the presently unknown Higgs mass M_H . In the low-mass region $M_H < 140$, the Higgs decays primary to $H \rightarrow b\bar{b}$, a challenging signature at a hadron collider. For this reason, the Tevatron sensitivity to a low-mass Higgs is primarily from channels producing a Higgs boson in association with a W or Z boson.

In this note, we present a search for ZH production in $\ell^+\ell^-b\bar{b}$ final states where ℓ is either a muon or an electron. The cross section times branching fraction for this process $\sigma(p\bar{p} \rightarrow ZH) \times B(H \rightarrow b\bar{b})$ is predicted to be 14 fb at $M_H = 100$ GeV falling to 0.75 fb at $M_H = 150$ GeV [1]. A Z -boson candidate is identified from a pair of reconstructed electrons or muons with requirements on transverse momentum p_T , and dilepton invariant mass $M_{\ell\ell}$ optimized for each channel as described below. Two specialized selections allow the reconstruction of one of the leptons with much looser criteria than used by most analyses, thus increasing the signal acceptance. Events are further required to have at least two jets with at least one of the jets originating from a b quark. To extract additional sensitivity to the signal process $ZH \rightarrow \ell^+\ell^-b\bar{b}$, a boosted decision tree discriminant [15] is trained to separate SM background from ZH signal events. The dominant backgrounds result from the associated production of a Z boson with jets, among which the non-resonant $Zb\bar{b}$ production is an irreducible background. The other backgrounds are $t\bar{t}$, WZ , ZZ , and multijet production with misidentified leptons.

II. DATA SAMPLE AND EVENT SELECTION

The DØ detector has a central-tracking system consisting of a silicon microstrip tracker (SMT) and a central fiber tracker located within a 2 T superconducting solenoidal magnet. The tracking coverage extends to pseudorapidity $|\eta| < 3$ with vertexing capability for $|\eta| < 2.5$. A liquid-argon and uranium-lead calorimeter has a central section covering $|\eta|$ up to ≈ 1.1 , and two endcap calorimeters that extend coverage to $|\eta| \approx 4.2$ [4]. The region $1.1 < |\eta| < 1.5$ is called the inter-cryostat region (ICR) and has limited coverage by the electromagnetic calorimeter. An outer muon system, at $|\eta| < 2$, consists of a layer of tracking detectors and scintillation trigger counters in front of 1.8 T toroids, followed by two similar muon detector layers outside of the toroids.

This analysis uses data collected between April 2002 and December 2008. The efficiency for the electrons from $Z \rightarrow e^+e^-$ decays to satisfy the online trigger is close to 100%. For $Z \rightarrow \mu^+\mu^-$ decays, the efficiency is approximately 95% and the trigger response has been modeled in the simulation. The integrated luminosity for the full dataset is found to be 4.2 fb^{-1} after data quality requirements. The dielectron and dimuon channels presented in this note use a subset of this data taken from June 2006 to December 2008 (Run IIb) with an integrated luminosity of 3.1 fb^{-1} . The results from a previous analysis [2] of the dielectron and dimuon channels are included to obtain a limit for the full Run II dataset. The new muon+track selection uses the full Run II dataset, while the new electron+ICR selection uses the Run IIb dataset.

Candidate events are selected beginning with the requirement that at least one primary vertex is reconstructed within 60 cm of the detector center along the beamline (z direction). The primary vertex must have at least three associated tracks. The events are also required to have at least two electrons or at least two muons as described below. In addition, at least two jets are required in each event, with $p_T > 20$ GeV for the leading jet, $p_T > 15$ GeV for the others, and $|\eta| < 2.5$ for all jets. A neural network b -tagging algorithm has been applied to separate b -quark jets from light-quark jets [5]. In the following subsections, details are given on the lepton and jet selections and on the b -tagging requirements.

A. Dielectron Selection

Events are required to have at least two electrons with $p_T > 15$ GeV identified in the central calorimeter, endcap calorimeter, or the inter-cryostat region. The electrons detected in the central calorimeter (CC) or in the endcap calorimeters (EC) with $|\eta| < 2.5$ are required to pass selection requirements based on the calorimeter shower shape, fraction of electromagnetic energy over hadronic energy, and isolation of the electron from nearby energy. In addition the electrons in the CC must match to a central track or produce an electron-like hit pattern in the tracker. These electrons are referred to as calorimeter electrons in this note. The electrons in the ICR are reconstructed as a tau-like narrow jet with a matching track. A neural network is used to differentiate such electrons from jets. These electrons are referred to as ICR electrons. The identification efficiencies for calorimeter electrons and ICR electrons are corrected

as a function of the pseudorapidity $\eta_{detector}$ and azimuthal angle ϕ of the electron. The notation $\eta_{detector}$ indicates that the pseudorapidity is measured with respect to the center of the DØ detector.

A Z candidate is required, reconstructed from two calorimeter electrons (dielectron sample) or a calorimeter electron and an ICR electron (electron+ICR sample). In the dielectron sample at least one of the electrons is required to be reconstructed in the CC. In the electron+ICR sample exactly one ICR electron and exactly one calorimeter electron in the CC or EC are required. The invariant mass of the electrons, M_{ee} , must be between 70 and 110 GeV.

B. Dimuon Selection

Events are required to have at least two opposite-sign muons identified either with the muon and tracking detectors or with the tracking detector alone. For identification with both detectors, each muon must have $p_T > 10$ GeV. Muons identified with only the tracking detector (μ_{track}) must have $p_T > 20$ GeV. For either case, the muon must have $|\eta_{detector}| < 2.0$ and the p_T is corrected using the beam spot position for muon tracks without SMT hits to improve track momentum resolution. In the simulation, the muon identification efficiency is corrected as a function of $\eta_{detector}$ and ϕ for each muon to match the efficiency measured in data control samples.

A Z candidate is required, reconstructed from two muons (dimuon sample) or a muon plus a track which fails the muon identification requirements (muon+track sample). To ensure the two data sets are orthogonal, the muon+track sample consists of events with one track-only muon and exactly one muon passing the full muon identification requirements. In both samples, the invariant mass of the muons, $M_{\mu\mu}$, must be between 70 and 130 GeV.

Muon isolation requirements are based on variables $\Delta R = \sqrt{(\Delta\eta)^2 + (\Delta\phi)^2}$ and scaled isolation $iso = (p_T^{cone} + E_T^{calorimeter})/p_T^{\mu}$, where p_T^{cone} is the sum of all tracks in a cone with $\Delta R < 0.5$ around and excluding the muon track, and $E_T^{calorimeter}$ is the sum of all calorimeter energy in a hollow cone around the muon from $0.1 < \Delta R < 0.4$. In the dimuon sample the product of the scaled isolation for the two muons is required to be less than 0.03. For the muon+track sample, the product scaled isolation must be less than < 0.01 . Additionally, the track-only muon must pass a scaled isolation requirement $iso(\mu_{track}) < 0.3$ and must be isolated from any other muon (μ) or jet (j) by $\Delta R(\mu_{track}, \mu) > 0.1$ and $\Delta R(\mu_{track}, j) > 0.5$.

C. Jet ID and b -jet Tagging

Jets are reconstructed using the Run II cone algorithm with $\Delta R = 0.5$ [6]. All jets are required to have $|\eta_{detector}| < 2.5$. The energy scale for jets is corrected for detector response, noise and the presence of multiple interactions, and energy deposited outside of the reconstructed jet cone. In the simulation, jet energies are smeared to reproduce the resolution observed in data. Energy scale corrections to the jets and leptons are propagated in the computation of the missing transverse energy \cancel{E}_T . For dielectron events, all jets are required to be isolated from both electrons by $\Delta R > 0.5$. Two jets are required in each event with the leading jet having $p_T > 20$ GeV, and all subsequent jets having $p_T > 15$ GeV. To reduce the impact from multiple interactions at high instantaneous luminosities, jets are also required to contain at least two reconstructed tracks that have been matched to the event primary vertex, referred to as vertex confirmation.

Jets are classified according to the output of an artificial neural network (NN) trained to use secondary vertex and track kinematic information to separate jets originating from b -quarks from those originating from light quarks. Two orthogonal b -tagged samples are selected according to the number of jets that pass a loose and tight cut on the b -tagging NN output variable. The single-tag (ST) requirement is that exactly one jet passes the tight NN cut while no additional jet passes the loose NN cut. The double-tag (DT) requirement is that at least two jets pass the loose NN cut. For each event, we associate exactly two jets with the Higgs-boson decay. In the ST sample, the tight-tagged jet and the highest- p_T untagged jet are selected. In the DT sample, the two highest- p_T loose-tagged jets are selected.

In simulation, we apply the probability that a jet of a given flavor would be tagged. This probability is measured from data as a function of jet kinematics. The b -tagging requirements are optimized to maximize the b -tagging efficiency while keeping the light-jet fake rate low. The resulting b -tagging efficiency for a loose tag is 72% in the central region ($|\eta| < 0.8$), for $p_T > 30$ GeV and the corresponding fake rate 4%. For a very tight tag the efficiency is 50% with a fake rate of 0.5%.

D. Multijet Background

The background contribution from multijet processes is estimated from data. The dielectron multijet sample consists of events with two electrons that fail the calorimeter shower-shape requirements imposed during the dielectron

selection. The ICR electrons are required to fail the artificial neural net discriminant cut imposed by electron+ICR selection. The dimuon multijet sample consists of events which fail the combined isolation requirement.

For the dielectron, electron+ICR, and dimuon samples the actual number of multijet events that pass the signal requirements is not the same as the number of events that pass the inverted requirements used to obtain the multijet samples. We determine the multijet normalization by fitting the dilepton invariant mass in data to shape templates from the multijet samples and SM background samples. The muon+track multijet sample consists of events where the muon and track-only muon have the same charge, and does not require normalization.

E. Simulated Event Samples

All non-multijet Standard Model backgrounds are estimated using a Monte Carlo simulation. Using the CTEQ6L1 [7] leading-order parton distribution function, we simulate the following physics processes to estimate the signal acceptance and the number of background events: $Z(\rightarrow \ell^+\ell^-)H(\rightarrow b\bar{b})$ by PYTHIA [10], $Z(\rightarrow \ell^+\ell^-)jj$ including $Z(\rightarrow \ell^+\ell^-)c\bar{c}$ and $Z(\rightarrow \ell^+\ell^-)b\bar{b}$ ($Z + HF$), and $t\bar{t} \rightarrow \ell^+\nu b\ell^-\bar{\nu}\bar{b}$ by ALPGEN [11], and inclusive ZZ , WZ , and WW by PYTHIA, where j stands for any light quark (uds). The samples generated by ALPGEN are interfaced with PYTHIA for parton showering and hadronization. All samples are processed using a detector simulation program based on GEANT [12], and the offline reconstruction algorithms.

The signal cross sections, as well as those for $t\bar{t}$, ZZ , WZ , and WW are taken from MCFM [13] and calculated at Next-to-Leading Order (NLO). For the ALPGEN samples, we use a matching procedure to avoid double counting the partons produced by ALPGEN and subsequently added by PYTHIA. In addition, NLO corrections are applied to the $Z + nj$, $Z + b\bar{b}$ and $Z + c\bar{c}$ samples, respectively, to account for the NLO cross sections of these processes (as calculated with MCFM) as compared to the Leading-Log cross sections from ALPGEN. The NLO calculations for $Z + b\bar{b}/c\bar{c}$ have a 30% uncertainty which we apply as a systematic uncertainty to these samples. Since the Z p_T distribution is poorly modeled in $Z + \text{jet}$ simulation, the simulated $Z + \text{jet}$ samples are reweighted according to the measured Z p_T spectrum before b -tagging. The dielectron and dimuon invariant mass distributions for data and background in the four channels after all reweighting are shown in Fig. 1. The simulation is corrected for the difference in efficiency for jet vertex confirmation with respect to the data. The two leading-jet η positions and their relative azimuthal angle $\Delta\phi(j, j)$ are poorly modeled by the ALPGEN simulation and are reweighted to account for this discrepancy. For ALPGEN Z backgrounds the η correction cancels the vertex confirmation correction, and so neither correction is applied. The luminosity profile and primary vertex distribution of the simulated events are reweighted to match the luminosity profile of the dielectron and dimuon data sample.

III. ANALYSIS

The event yields for all of the four channels are shown in Tables I-IV, where the pre-selection includes all event selection requirements on both the leptons and jets, except for the dilepton invariant-mass cut and the b -tagging requirements. There is good agreement between the background prediction and the yields observed in data. Furthermore, it is seen that the inclusion of ICR electrons and track-only muons adds roughly 15% signal acceptance to the dielectron and dimuon channels, respectively. We proceed to use a multivariate technique, described in Section III B, to further separate the signal from the background.

A. Kinematic Fitting

The dielectron, dimuon and muon+track channels apply a kinematic fit of the Z boson and jets. The kinematic fit allows the energies and angles of the leptons and jets to fluctuate according to the detector resolution, to minimize a χ^2 under the following constraints:

- The dilepton mass is constrained to the Z mass (M_Z) within the Z width (Γ_Z): $M_{\ell\ell} = M_Z \pm \Gamma_Z$.
- The vector transverse momentum of the Zjj system is constrained to zero with a Gaussian width of 7 GeV.

B. Multivariate Discriminant Analysis

In order to take full advantage of the kinematic information in the data, we use a multivariate discriminant analysis to search for the associated ZH production. BDT discriminants are trained for each channel (dielectron: separately

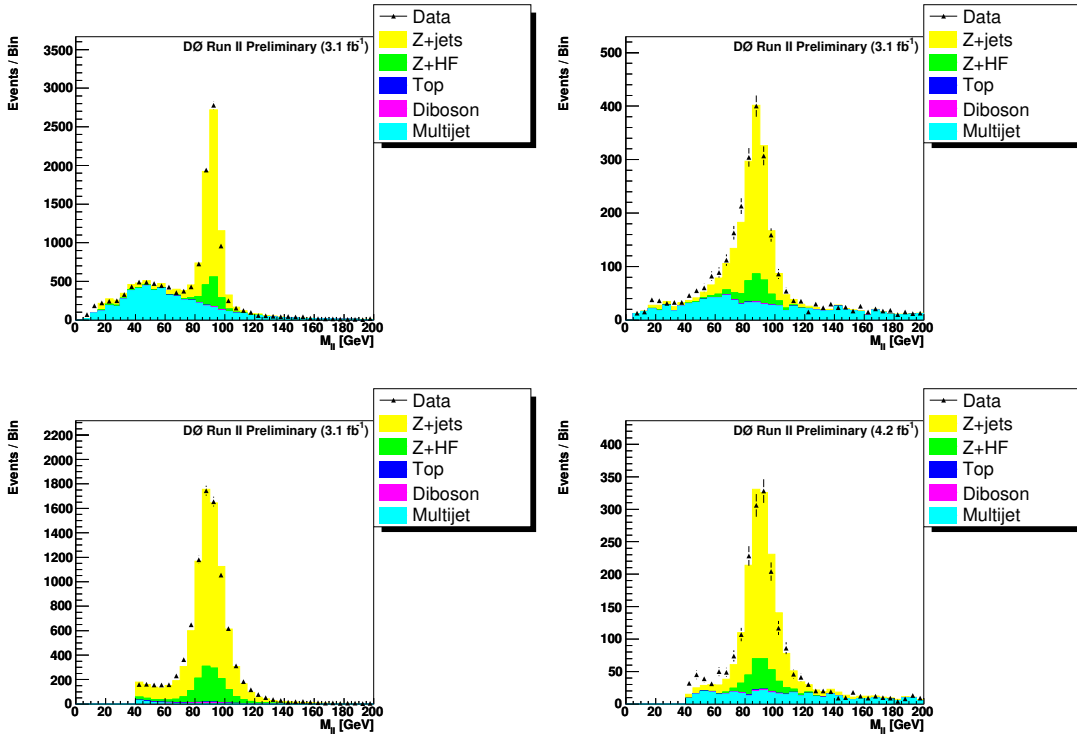


FIG. 1: The dielectron (top, left), electron+ICR electron (top, right), dimuon (bottom, left) and muon+track (bottom, right) invariant mass distributions prior to the b-tagging requirement.

	pre-selection	$70 < M_{ee} < 110$ GeV	1 tight b-tag	2 loose b-tags
Data	12747	7610	201	131
Bkg	12926 ± 73	7900 ± 44	198.3 ± 1.3	119.0 ± 0.9
$ZH(115)$	2.09 ± 0.02	1.98 ± 0.02	0.52 ± 0.005	0.69 ± 0.007
Multijet	5303 ± 62	1368 ± 25	32.1 ± 0.6	16.6 ± 0.3
Zjj	6301 ± 37	5458 ± 35	29.6 ± 0.2	21.8 ± 0.1
$Zb\bar{b}$	352.6 ± 3.5	308.3 ± 3.3	80.4 ± 1.0	45.7 ± 0.8
$Zc\bar{c}$	798.0 ± 7.3	663.7 ± 6.6	45.5 ± 0.5	22.5 ± 0.3
ZZ	36.4 ± 0.6	32.6 ± 0.5	2.46 ± 0.08	2.47 ± 0.10
WZ	43.8 ± 0.9	40.7 ± 0.9	1.53 ± 0.05	0.61 ± 0.02
WW	9.42 ± 0.74	2.97 ± 0.40	0.096 ± 0.035	0.028 ± 0.007
$t\bar{t}$	81.9 ± 0.5	25.5 ± 0.3	6.58 ± 0.08	9.21 ± 0.12

TABLE I: The numbers of events and statistical uncertainties in the dielectron channel after each requirement for data, various background processes and ZH signal, where the mass of the Higgs boson is $m_H = 115$ GeV.

for the CC-CC and CC-EC configurations, electron+ICR electron, dimuon, and muon+track), at each Higgs mass point (100-150 GeV in 5 GeV steps) and for the single-tag and double-tag samples separately. In each channel, we use an optimized subset of the following variables that fall into 5 categories:

- $\eta(b, b)$, M_{bb} for jets assumed to be massless, $M_T(b, b)$ of the dijet system and the transverse boost of the Zjj system.
- the dijet invariant mass M_{bb} , the dijet invariant mass assuming massless jets, the transverse momentum, p_T^{bb} , of the dijet system, the dijet transverse mass $M_T(b, b)$, the $\Delta\eta$ and the opening azimuthal angle ($\Delta\phi(b, b)$) between the b -jet candidates, the p_T and η of the leading- p_T and second b -jet candidate.
- $M_{\ell\ell}$, rapidity and pseudo-rapidity of the Z , the opening angle of the dilepton pair ($\Delta\phi(l, l)$), the $\Delta R(l, l)$, collinearity and pseudo-acollinearity of the two leptons

	pre-selection	$70 < M_{ee} < 110$ GeV	1 tight b-tag	2 loose b-tags
Data	2510	1686	44	34
Bkg	2379 ± 39	1651 ± 23	40.0 ± 0.7	25.2 ± 0.4
$ZH(115)$	0.38 ± 0.01	0.33 ± 0.001	0.09 ± 0.002	0.12 ± 0.003
Multijet	741 ± 33	226 ± 13	4.8 ± 0.6	2.9 ± 0.6
Zjj	1372 ± 18	1203 ± 19	6.7 ± 0.1	5.0 ± 0.08
$Zb\bar{b}$	74.2 ± 1.2	63.7 ± 1.6	16.9 ± 0.5	9.9 ± 0.3
$Zc\bar{c}$	162 ± 2.8	139 ± 4.4	9.7 ± 0.3	5.0 ± 0.2
ZZ	7.6 ± 0.2	6.5 ± 0.2	0.48 ± 0.01	0.60 ± 0.02
WZ	9.4 ± 0.4	8.2 ± 0.4	0.30 ± 0.01	0.11 ± 0.004
WW	1.3 ± 0.3	0.36 ± 0.10	0.01 ± 0.003	0.001 ± 0.002
$t\bar{t}$	11.0 ± 0.1	4.3 ± 0.07	1.14 ± 0.02	1.68 ± 0.03

TABLE II: The numbers of events and statistical uncertainties in the electron+ICR electron channel after each requirement for data, various background processes and ZH signal, where the mass of the Higgs boson is $m_h = 115$ GeV.

	pre-selection	$70 < M_{\mu\mu} < 130$ GeV	1 tight b-tag	2 loose b-tags
Data	9304	8004	217	161
Bkg	9072 ± 39	7922 ± 37	229.5 ± 1.3	148.8 ± 1.0
$ZH(115)$	2.542 ± 0.020	2.361 ± 0.019	0.6114 ± 0.0051	0.8560 ± 0.0079
Multijet	83.86 ± 0.68	12.71 ± 0.27	1.831 ± 0.044	1.866 ± 0.035
Zjj	7285 ± 38	6435 ± 36	35.36 ± 0.20	27.34 ± 0.14
$Zb\bar{b}$	465.4 ± 3.9	422.0 ± 3.7	112.3 ± 1.1	66.44 ± 0.93
$Zc\bar{c}$	1032 ± 8.1	915.0 ± 7.5	63.92 ± 0.63	32.59 ± 0.39
ZZ	47.63 ± 0.67	43.25 ± 0.63	3.41 ± 0.10	3.72 ± 0.14
WZ	51.38 ± 0.97	47.20 ± 0.92	1.844 ± 0.058	0.793 ± 0.029
WW	12.25 ± 0.82	4.95 ± 0.52	0.149 ± 0.024	0.072 ± 0.014
$t\bar{t}$	94.39 ± 0.52	41.87 ± 0.35	10.735 ± 0.092	15.97 ± 0.15

TABLE III: The numbers of events and statistical uncertainties in the dimuon sample after each requirement for data, various background processes and ZH signal, where the mass of the Higgs boson is $M_H = 115$ GeV.

- $\Delta\phi$ between the Z and dijet system, the $\Delta\phi$ between the Z and the \cancel{E}_T .
- The \cancel{E}_T , $\cos(\theta^*)$, $\cos(\chi^*)$

The angles θ^* and χ^* are spin correlation variables proposed in [8]. These variables were derived to separate WH from $Wb\bar{b}$ samples [9], but have been found to provide useful discrimination in the ZH search as well.

The input distributions of several of the most significant variables for the BDT discriminant are shown in Figs. 2–6. The BDT output distributions for the four channels and two b-tagged samples for a Higgs mass of 115 GeV are shown in Figs. 7 and 8.

	pre-selection	$70 < M_{\mu\mu} < 130$ GeV	1 tight b-tag	2 loose b-tags
Data	2243	1587	56	38
Bkg	2208 ± 27	1637 ± 18	56.76 ± 0.97	31.53 ± 0.76
$ZH(115)$	0.4421 ± 0.0078	0.4122 ± 0.0075	0.1157 ± 0.0021	0.1323 ± 0.0027
Multijet	609 ± 25	187 ± 14	10.79 ± 0.79	8.29 ± 0.67
Zjj	1336 ± 11	1205 ± 11	16.10 ± 0.39	6.81 ± 0.19
$Zb\bar{b}$	71.0 ± 1.3	68.8 ± 1.2	17.42 ± 0.34	8.97 ± 0.26
$Zc\bar{c}$	152.7 ± 2.6	148.1 ± 2.5	9.27 ± 0.20	4.17 ± 0.12
ZZ	3.28 ± 0.41	1.50 ± 0.30	0.048 ± 0.018	0.0149 ± 0.0039
WZ	11.29 ± 0.17	10.63 ± 0.17	0.389 ± 0.011	0.1343 ± 0.0036
WW	8.53 ± 0.22	7.97 ± 0.21	0.617 ± 0.034	0.560 ± 0.038
$t\bar{t}$	15.84 ± 0.41	7.65 ± 0.29	2.133 ± 0.078	2.60 ± 0.11

TABLE IV: The numbers of events and statistical uncertainties in the muon+track sample after each requirement for data, various background processes and ZH signal, where the mass of the Higgs boson is $M_H = 115$ GeV.

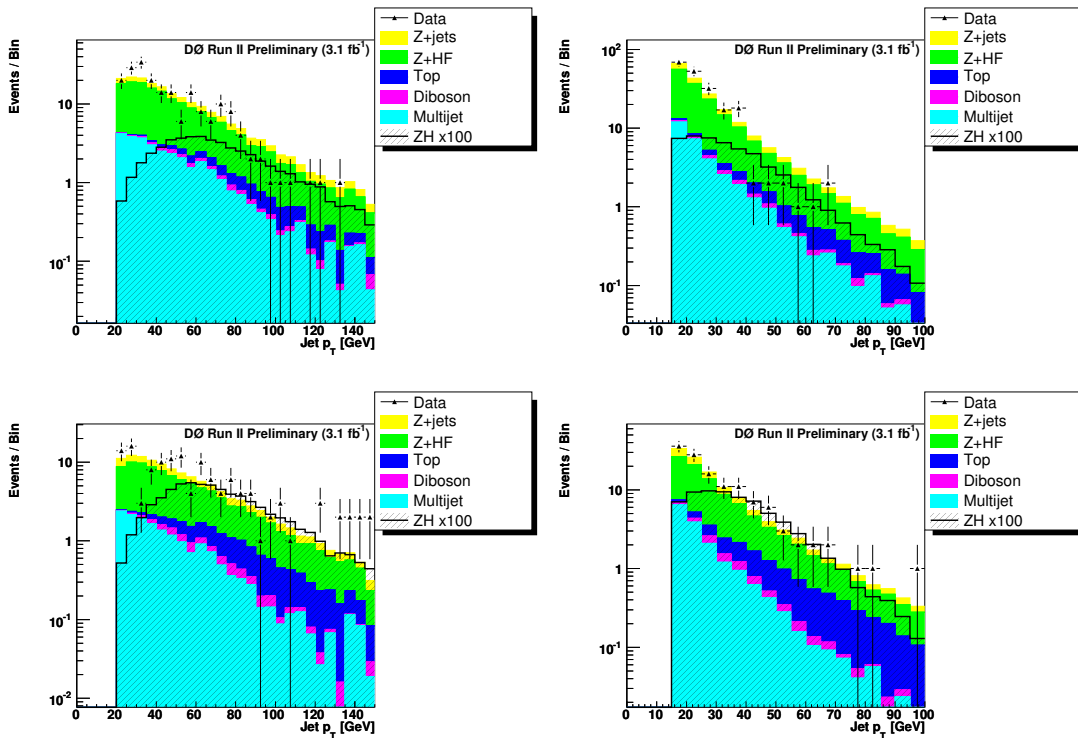


FIG. 2: The leading jet p_T (left column) and the second-leading jet p_T (right column) distributions in the dielectron sample. The top and bottom rows show the single- and double- tag samples, respectively.

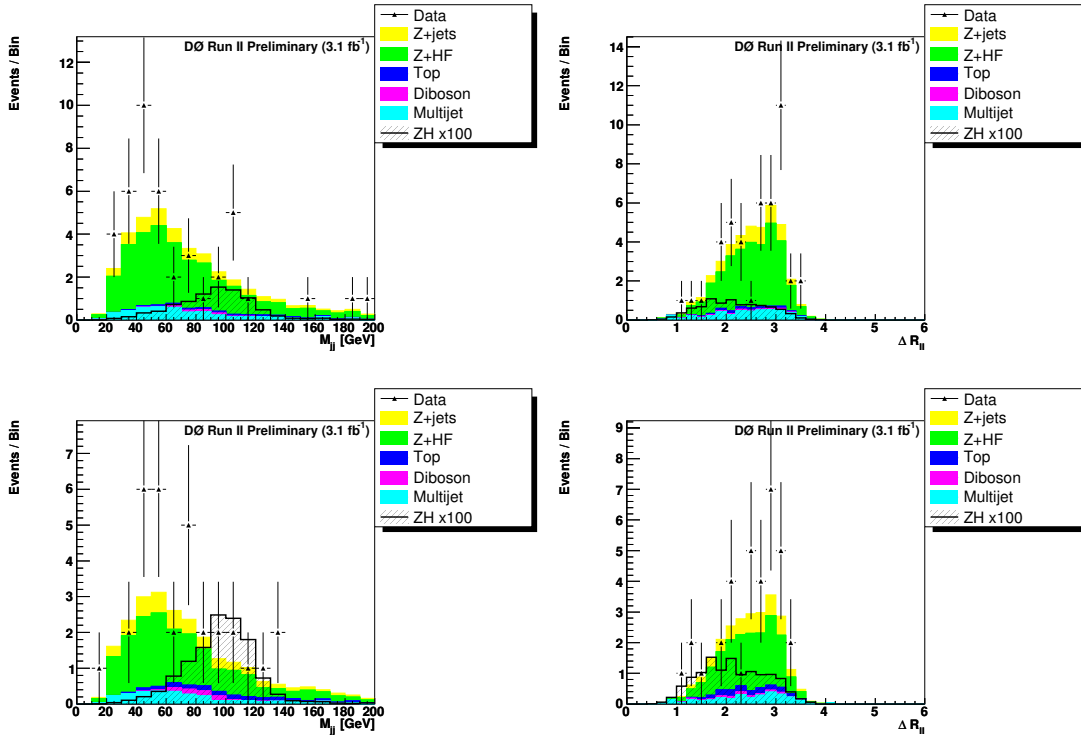


FIG. 3: The dijet invariant mass (left column) and the $\Delta R(\ell, \ell)$ of the electrons in the electron+ICR electron sample. The top and bottom rows show the single- and double- tag samples, respectively.

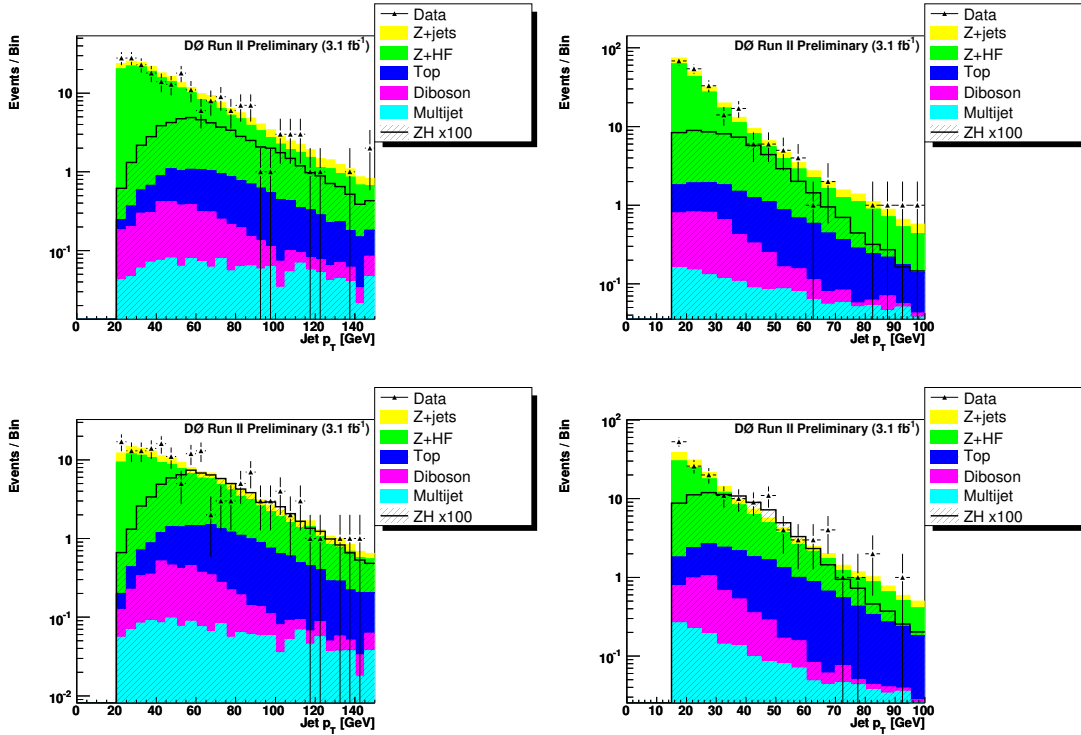


FIG. 4: The leading jet p_T (left column) and the second-leading jet p_T (right column) distributions in the dimuon sample. The top and bottom rows show the single- and double- tag samples, respectively.

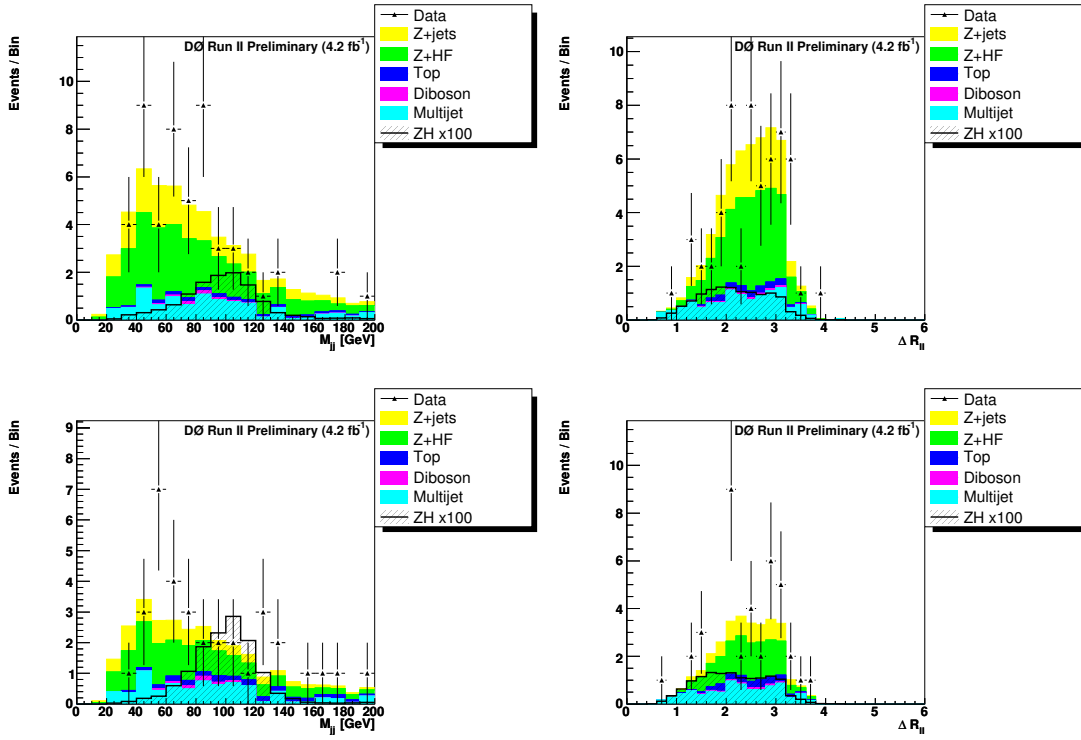


FIG. 5: The dijet invariant mass (left column) and the $\Delta R(\ell, \ell)$ of the muons in the muon+track sample. The top and bottom rows show the single- and double- tags sample, respectively.

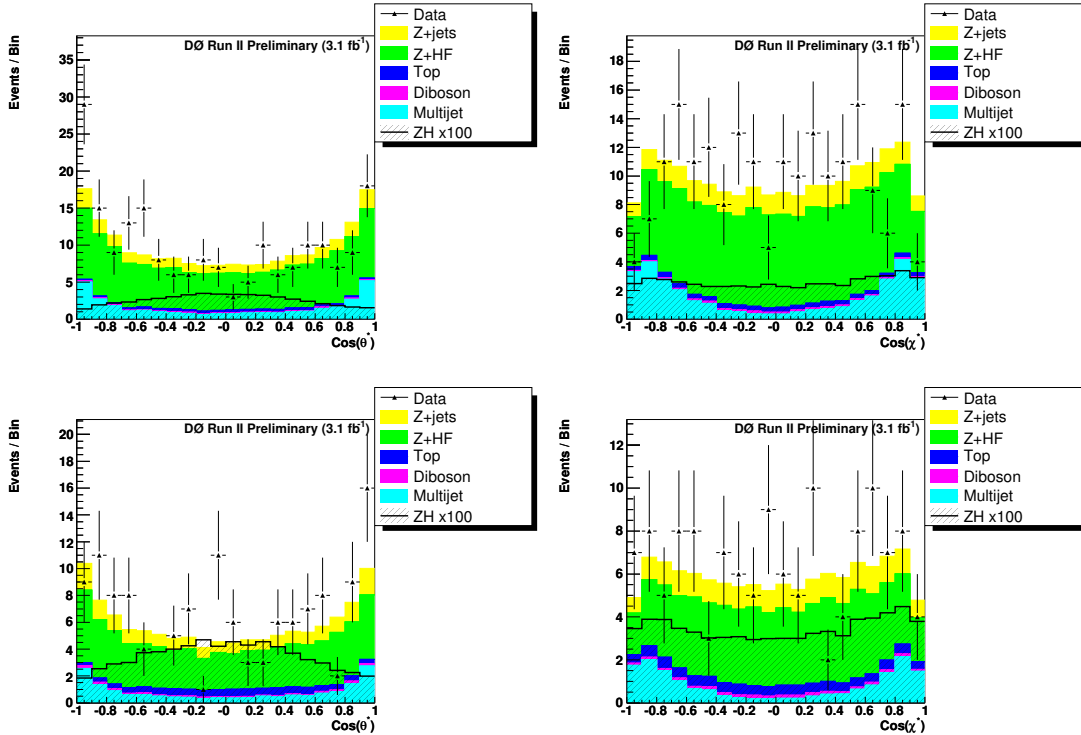


FIG. 6: Distributions of $\cos(\theta^*)$ (left column) and $\cos(\chi^*)$ (right column) in the dielectron sample. The top and bottom rows show the single- and double- tag samples, respectively.

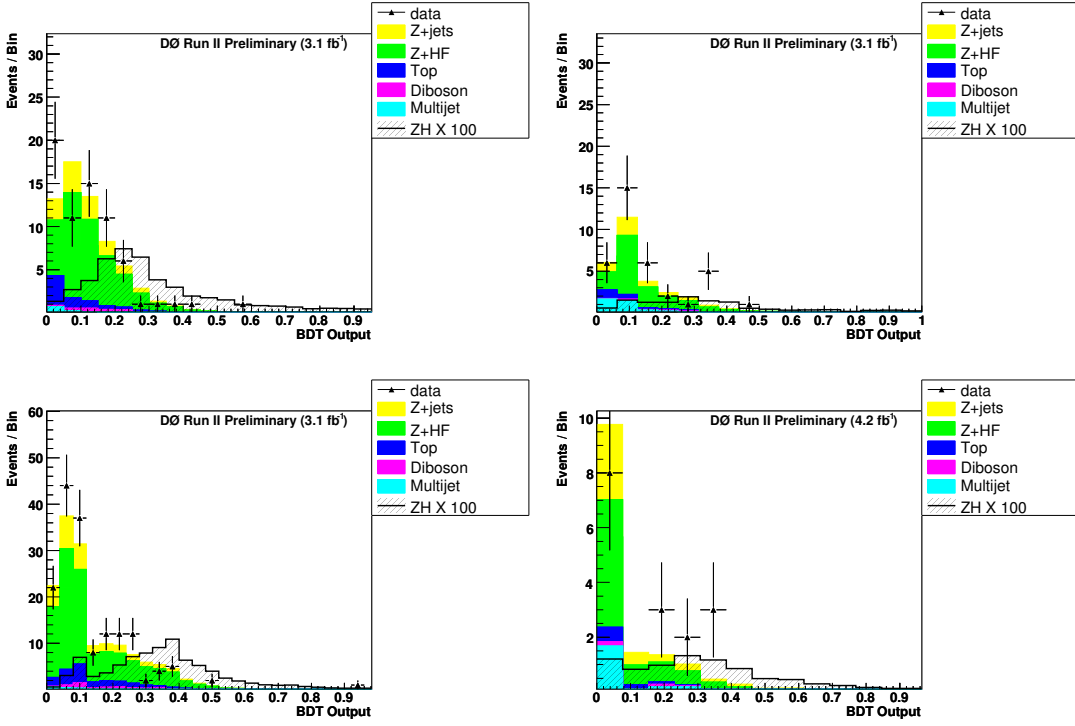


FIG. 7: The boosted decision tree output for the double b-tag sample in the four channels: dielectron (top, left), electron+ICR electron (top, right), dimuon samples (bottom, left) and muon+track (bottom, right). The multivariate discriminants are trained for the Higgs mass of 115 GeV.

C. Systematic Uncertainties

The systematic uncertainties due to data/MC differences in the distributions of the dijet invariant mass, and of the \cancel{E}_T are taken into account in the limit calculation program, considering also the effects on the shape of the multivariate output. Similarly the uncertainties due to the jet energy scale, the jet track matching efficiency correction, b-tagging probabilities, Z - p_T reweighting, vertex confirmation scale factor, jet η reweighting, and $\Delta\phi(j, j)$ reweighting are considered by generating the multivariate discriminant output for MC samples with $\pm 1\sigma$ variations from the central values of the relevant parameters.

Other systematic uncertainties included in the calculation are the uncertainties for the luminosity measurement, the electron identification, the muon identification, the theoretical cross sections for the background processes and the estimate for the multijet background. These uncertainties affect only the overall normalization of each background sample. We use 6.1% for the uncertainty of the luminosity measurement [16]. Based on the uncertainties for the correction factors for the electron selection, we assign a 2% systematic uncertainty. The uncertainty on the corrections to the muon selection efficiency is 2%. The uncertainty for the multijet background is taken from the uncertainty on the multijet scale factor and is estimated to be 22% for the dielectron sample and 50% for the dimuon sample. Uncertainties of 10% are assigned to the theoretical cross sections for $Z + jj$ [14] and $t\bar{t}$ processes, 7% for diboson processes, and 30% for $Z + b\bar{b}/c\bar{c}$ processes.

D. Results

We set limits on the ZH cross section using a modified frequentist (CLs) method using a log-likelihood test statistic [17, 18]. The histograms of the BDT output for the single-tag and the double-tag samples in each channel are the input for the limit setting program. The histograms for the shape dependent systematic uncertainties in Section III C are used in the program, along with the constant systematic uncertainties. The impact of the systematics is minimized using a profile likelihood technique [18].

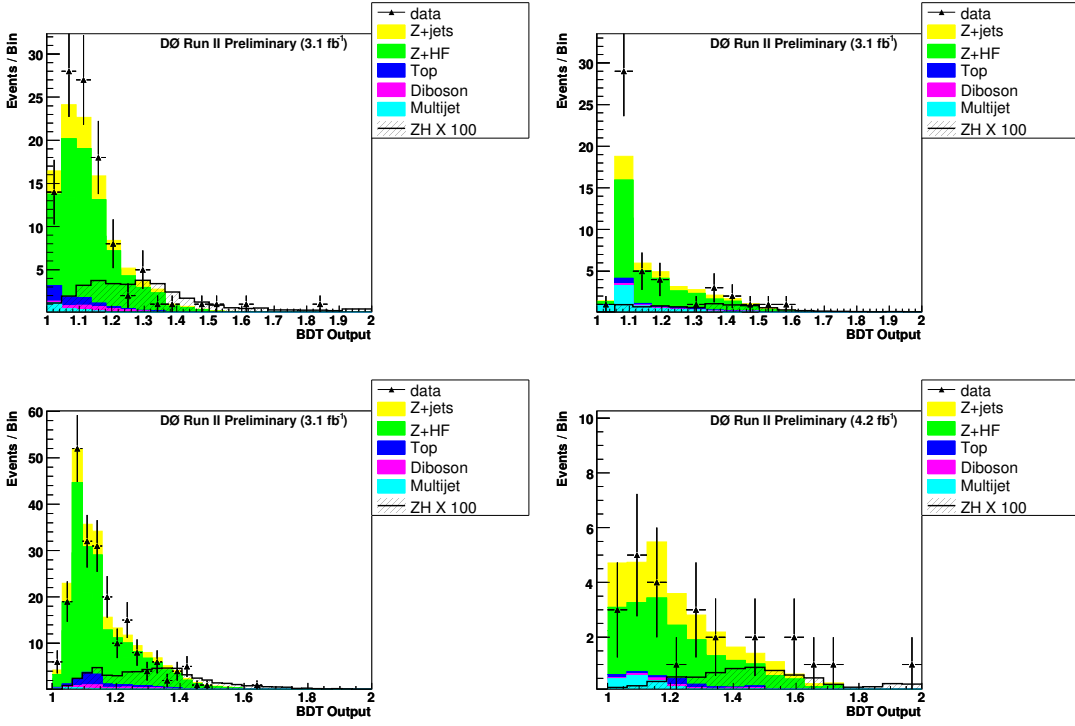


FIG. 8: The boosted decision tree output for the single b-tag sample in the four channels: dielectron (top, left), electron+ICR electron (top, right), dimuon samples (bottom, left) and muon+track (bottom, right). The multivariate discriminants are trained for the Higgs mass of 115 GeV.

Table V shows the expected and observed ratio of the cross section limit to the Standard Model cross-section for each channel at each analyzed mass point. Also shown are the combined limits including a previous analysis [2] of the dielectron and dimuon channels using data not included in this analysis. These combined limits and the corresponding log-likelihood ratios are displayed in Fig. 9. The observed limits on the cross section over the SM value ($\frac{\sigma_{limit}}{\sigma_{SM}}$) at $M_H=115$ GeV is about 19 for the dielectron channel, 68 for the electron+ICR channel, 13 times for the dimuon channel, and 78 for the muon+track channel. Combining the electron and muon channels for the full Run II dataset, the observed cross section limit for a Higgs mass of 115 GeV is 9.1 times the Standard Model prediction.

M_H (GeV)	Run IIb $\mu\mu$		Run IIb ee		Full Run II μ +track		Run IIb e +ICR		Full Run II combination	
	Exp/SM	Obs/SM	Exp/SM	Obs/SM	Exp/SM	Obs/SM	Exp/SM	Obs/SM	Exp/SM	Obs/SM
100	9.29	7.7	11.4	18.5	38.6	43.4	42.3	38.0	6.0	4.3
105	11.1	9.0	12.6	19.2	43.2	45.3	45.6	53.8	6.4	6.6
110	12.8	10.9	14.6	17.0	46.7	69.7	50.2	56.3	7.3	6.5
115	14.7	13.3	15.3	18.7	50.4	78.0	57.0	68.2	8.0	9.1
120	17.7	14.2	19.2	23.9	63.4	75.2	68.8	87.7	9.9	11.4
125	20.7	19.5	20.9	27.0	74.1	86.7	85.5	91.2	11.2	13.5
130	26.2	25.6	27.4	42.4	90.4	120	102	130	14.5	20.3
135	34.2	44.1	34.9	43.6	126	142	146	159	18.7	27.5
140	47.9	62.0	50.3	73.2	167	188	198	232	26.2	40.8
145	64.9	91.5	69.2	85.5	250	252	269	243	37.5	52.7
150	104	129.3	114	123	428	331	457	380	58.3	67.6

TABLE V: Measured and expected limits on the Standard Model Higgs production cross-section in the individual $ZH \rightarrow \ell\ell b\bar{b}$ channels after combining the ST and DT samples using the boosted decision tree output as a discriminant. The last two columns show the full combined limits including a previous analysis [2].

IV. SUMMARY

A search for a Higgs boson produced in association with a Z boson in $p\bar{p}$ collisions at $\sqrt{s} = 1.96$ TeV at the Fermilab Tevatron collider is performed, using 4.2 fb^{-1} of data. Events with a $Z \rightarrow \ell^+\ell^-$ and two jets where at least one jet is b -tagged are selected. The observed data are consistent with the expected background. Upper limits on the ZH production cross section are set for Higgs masses between 100 and 150 GeV. The limits on the cross section for a Higgs boson of mass of 115 GeV are about 9.1 times the Standard Model prediction from the combination of the dielectron and dimuon Run II analyses.

Acknowledgments

We thank the staffs at Fermilab and collaborating institutions, and acknowledge support from the DOE and NSF (USA); CEA and CNRS/IN2P3 (France); FASI, Rosatom and RFBR (Russia); CAPES, CNPq, FAPERJ, FAPESP and FUNDUNESP (Brazil); DAE and DST (India); Colciencias (Colombia); CONACyT (Mexico); KRF and KOSEF (Korea); CONICET and UBACyT (Argentina); FOM (The Netherlands); STFC (United Kingdom); MSMT and GACR (Czech Republic); CRC Program, CFI, NSERC and WestGrid Project (Canada); BMBF and DFG (Germany); SFI (Ireland); The Swedish Research Council (Sweden); CAS and CNSF (China); and the Alexander von Humboldt Foundation.

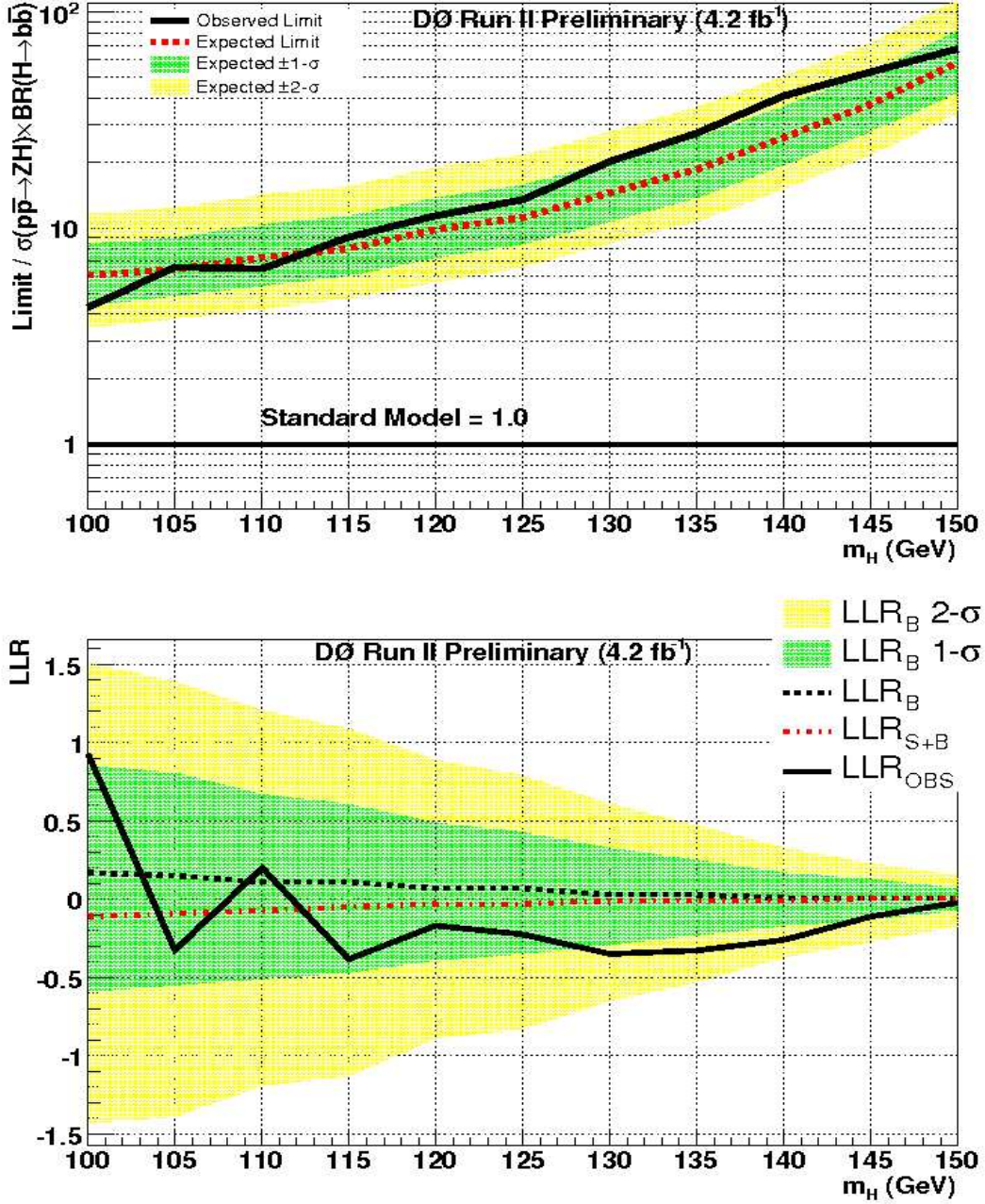


FIG. 9: The ZH production cross-section limits determined from combining the output of the boosted decision tree analysis in the ST and DT samples for each of the dielectron, electron+ICR, dimuon and muon+track channels, including limits obtained in a previous analysis [2] of the dielectron and dimuon channels of 1.1 fb⁻¹ integrated luminosity not included in this analysis.

-
- [1] T. Han and S. Willenbrock, Phys. Lett. **B273** 167 (1991). A.Djouadi, J.Kalinowski and M.Spira, Comp. Phys. Commun. **108 C**, 56 (1998).
 - [2] V.M. Abazov *et al.* (DØ Collaboration), DØ Note 5482-CONF (2007).
 - [3] V.M. Abazov *et al.* (DØ Collaboration), Nucl. Instrum. Methods Phys. Res. A **565**, 463 (2006).
 - [4] S. Abachi, *et al.*, Nucl. Instrum. Methods Phys. Res. A **338**, 185 (1994).
 - [5] T. Scanlon, FERMILAB-THESIS-2006-43.
 - [6] G. C. Blazey *et al.*, in *Proceedings of the Workshop: "QCD and Weak Boson Physics in Run II,"* edited by U. Baur, R. K. Ellis, and D. Zeppenfeld, (Fermilab, Batavia, IL, 2000) p. 47; see Sec. 3.5 for details.
 - [7] J. Pumplin *et al.*, J. High Energy Phys. **07**, 012 (2002).
 - [8] S. Parke and S. Veseli, Phys Rev D **60**, 093003 (1999).
 - [9] G. Bernardi *et al.*, DØ Note 5714 (2008).
 - [10] T. Sjostrand *et al.*, Comput. Phys. Commun. **135**, 238 (2001).
 - [11] M. L. Mangano *et al.*, J. High Energy Phys. **0307**, 001 (2003).
 - [12] R. Brun, F. Carminati, CERN Program Library Long Writeup W5013 (1993).
 - [13] J. Campbell and R. K. Ellis, MCFM, *Monte Carlo for FeMtobarn processes*, <http://mcfm.fnal.gov/>.
 - [14] J. Campbell and R. K. Ellis, Phys. Rev. D **65**, 113007 (2002).
 - [15] T. Hastie, R. Tibshirani, and J. Friedman, "The Elements of Statistical Learning" Springer (2001)
 - [16] T. Andeen *et al.*, FERMILAB-TM-2365 (2007).
 - [17] T. Junk, Nucl. Instrum. Methods Phys. Res., Sect. A **434**, 435 (1999); A. L. Read, Workshop on Confidence Limits, CERN-OPEN-2000-205 (2000).
 - [18] W. Fisher, FERMILAB-TM-2386-E (2007).